IEEE Access
Multidisciplinary ⋮ Rapid Review ⋮ Open Access Journal

Received 7 March 2024, accepted 17 March 2024, date of publication 21 March 2024, date of current version 27 March 2024.

Digital Object Identifier 10.1109/ACCESS.2024.3380370

RESEARCH ARTICLE

Design and Analysis of Interdigital Electrode Parallel Layout of Multilayer SAW Devices

XU MENG[1] AND ZHIPENG LI[2]

[1]College of Automotive Engineering, Changzhou Institute of Technology, Changzhou 213028, China
[2]School of Traffic and Transportation, Northeast Forestry University, Harbin 150040, China

Corresponding author: Xu Meng (Mengx@czu.cn)

This work was supported in part by the National Natural Science Foundation of China under Grant 52175497, and in part by the Key Research and Development Program of Heilongjiang Province in China under Grant JD22A014.

ABSTRACT To obtain high-frequency SAW devices, the interdigital transducer electrodes are prepared narrower and the electrode spacing is smaller, which leads to higher cost and lower reliability of high-frequency SAW devices. In this paper, two other interdigital electrode parallel layout structures are designed based on the traditional IDT flat layer layout structure, and the influence of the three different IDT electrode layout structures on the SAW device of $LiNbO_3$/Diamond/Si multilayer structure is studied by COMSOL Multiphysics. The results show that the designed multi-layer structure SAW device can successfully excite SAW with superior performance, and the parallel layout structure of the interdigital electrode can reduce the lateral size of SAW device, which provides a new idea and direction for the miniaturization of the SAW devices.

INDEX TERMS Design optimization, finite element analysis (FEA), interdigital transducer (IDT), multilayer structure, surface acoustic wave (SAW).

I. INTRODUCTION

With the wide application of wireless communication technology and the rapid development of sensor technology, SAW (surface acoustic wave) devices have received extensive attention and application in academia and industry [1], [2], [3], [4].

At present, some scholars have begun to use the structure and layout of IDT to improve the performance of SAW devices. Reference [5] studied the performance of surface acoustic wave devices using AlN/diamond/Si layered substrates and embedded interdigital transducers. Reference [6] proposed a double-sided IDT structure to enhance the driving capability of SAW devices. Reference [7] utilized a novel TIDT structure to apply SAW devices to metal inspection and expanded their application areas. Reference [8] combined the dispersion theory of aluminum plates and the design principle of IDT to design an all-around flexible circular PVDF interdigital transducer for structural health detection. Reference [9] proposed a multi-layer torque sensor for IDT/128°Y-X lithium niobate/diamond/Si (100) SAW devices and studied its performance. Reference [10] proposed a sensing method for extremely high temperatures using an Al_2O_3/IDT/AlN/Metal/Si composite surface acoustic wave device structure. Reference [11] proposed a model reduction (MOR) technique based on finite element and periodic boundary conditions, which can be used without reducing computational accuracy. Reference [12] proposed a high-frequency surface acoustic wave resonator based on a sandwich interdigital transducer, which adopted a multi-layer structure of diamond/AlN/IDT/AlN/diamond. Reference [13] used the finite element method to study the effects of different IDT layouts on the frequency and electromechanical coupling factor of SAW device structures.

In summary, there is no detailed study on the layered arrangement of IDTs currently. The paper uses $LiNbO_3$/diamond/Si multilayer structure as the main structure and different Mo electrode layered arrangements for simulation analysis to study their impact on the performance of multi-layer SAW devices.

II. MODELING AND SIMULATION

The interdigital transducer (IDT) is an important part of the SAW device, which is mainly used to excite and detect

The associate editor coordinating the review of this manuscript and approving it for publication was Norbert Herencsar.

SAW. It consists of two sets of interdigital electrodes and two sides of the bus bar, as shown in Figure 1. The characteristic frequency of the SAW device is inversely correlated with the width of the IDT interdigital electrode, that is, the narrower the width, the higher the working frequency of the SAW device. However, due to the high preparation cost, poor seismic capacity, and high temperature melting problem, it is mainly studied by weighting method [14], [15], [16].

The multilayer SAW device is coated with several layers of dielectric film on the substrate, and a reasonable combination of dielectric films can optimize the performance of the substrate material, which provides a new method for the development of SAW devices that meet more requirements [17]. The multi-layer SAW device designed in this paper is composed of a lithium niobate ($LiNbO_3$) film layer, diamond film layer, and silicon (Si) substrate layer, and it is simulated and analyzed by using different molybdenum (Mo) electrode layer layout structures.

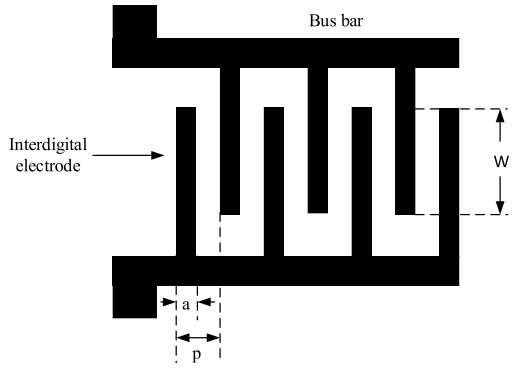

FIGURE 1. Schematic diagram of IDT structure.

Due to silicon (Si) is compatible with the manufacturing process of integrated circuits (IC) and the cost is low, silicon (Si) is selected as the substrate material of multilayer structures. Diamond has high-temperature resistance, strong structural stability, and high sound velocity [18], so diamond is selected as the growth layer material sandwiched between the substrate and the piezoelectric film. The electromechanical coupling coefficient of $LiNbO_3$ film has obvious advantages over AlN film and ZnO film. Therefore, the $LiNbO_3$ / Diamond structure can simultaneously obtain high phase velocity and high electromechanical coupling coefficient [19]. The perfectly matched layer (PML) is placed at the bottom of the Si substrate to avoid wave reflection from the bottom. The height of each layer is recorded as h_{IDT}, h_{LN}, h_{DIA}, h_{Si} and h_{PML}.

Based on this, three SAW device models are designed in this paper. As shown in Figure 2, the three structural forms of (a), (b), and (c) in the figure are Mo electrode flat layer layout structure, Mo electrode stagger layer layout structure, and Mo electrode cross-layer layout structure, respectively. The finite element calculation is carried out by COMSOL Multiphysics, and the boundary conditions and structural parameters of the finite element analysis are shown in Table 1 and Table 2 respectively.

TABLE 1. Symbols and parameter values of globally defined parameters.

Parameter name	Parameter symbolic	Parameter value
Wavelength	λ	4 μm
Electrode spacing 1	S_1	0.5 μm
Electrode spacing 2	S_2	1 μm
Electrode center distance	P	2 μm
Model width	W	8 μm
IDT height	h_{IDT}	0.2 μm
IDT width	d	1 μm
$LiNbO_3$ thickness	h_{LN}	2 μm
Diamond thickness	h_{DIA}	2 μm
Silicon thickness	h_{Si}	12 μm
PML thickness	h_{PML}	2 μm
euler angle α	Alpha	0 deg
euler angle β	Beta	0 deg
euler angle γ	Gamma	0 deg

TABLE 2. Boundary condition of the FEM analysis.

Boundary	Mechanical boundary condition	Electrical boundary condition
Electrode 2、Electrode 4	Free	1V
Electrode 1、Electrode 3	Free	0V
Γ_1、Γ_2、Γ_3、Γ_4	Free	Free
Γ_5	Fixed	Ground
Γ_{L1}、Γ_{L2}、Γ_{L3}、Γ_{L4}	Periodical boundary condition	
Γ_{R1}、Γ_{R2}、Γ_{R3}、Γ_{R4}	Periodical boundary condition	

The coordinate system of the piezoelectric material adopts the Euler angle (α, β, γ), and the Euler angle of the $LiNbO_3$ film material is set to (0°, 0°, 90°). SAW is mainly concentrated in the $LiNbO_3$ film, and some surface acoustic waves will penetrate the $LiNbO_3$ film into the Diamond film layer, so the mesh is gradually sparse from top to bottom, and the ultra-fine mesh is mainly concentrated on the surface of the interdigital electrode and the $LiNbO_3$ film layer.

For each SAW vibration mode, there are two vibration modes, and the characteristic frequency can be expressed as:

$$f_0 = \frac{(f_{sc-} + f_{sc+})}{2} \tag{1}$$

where, f_{sc-} is the symmetric modal frequency, f_{sc+} is the anti-symmetric modal frequency. The electromechanical coupling coefficient K^2 is derived from the equivalent circuit analysis as follows:

$$K^2 = \frac{\pi f_{sc-}/2f_{sc+}}{\tan\left(\pi f_{sc-}/2f_{sc+}\right)} \tag{2}$$

III. RESULTS AND DISCUSSION

A. VIBRATION MODAL

The first-order mode is selected as the main mode, and the displacement distribution of the symmetric mode (left) and the anti-symmetric mode (right) of the three models is calculated as shown in Figure 3. The characteristic frequency of the Mo electrode flat layer layout structure model is 1.042 GHz, the characteristic frequency of the Mo electrode staggered

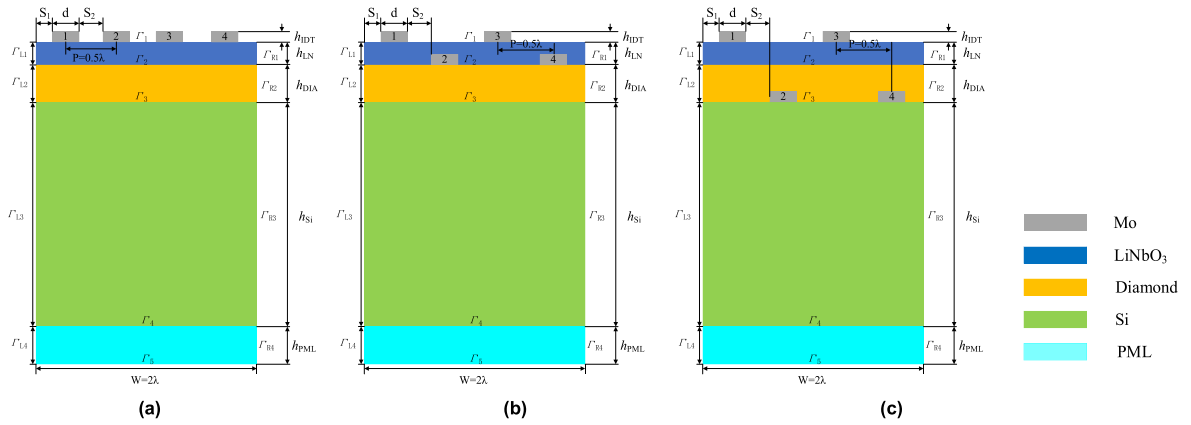

FIGURE 2. Three layout structures: (a) Flat layer layout structure; (b) Stagger layer layout structure; (c) Cross layer layout structure.

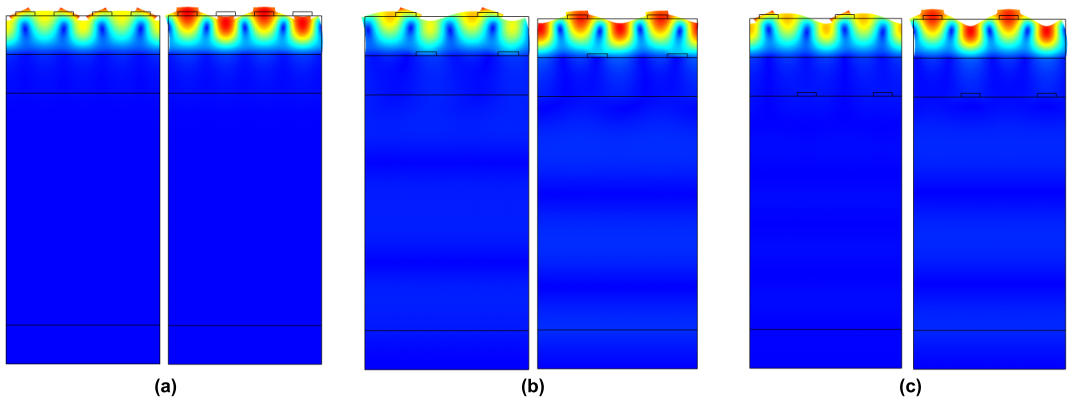

FIGURE 3. First-order symmetric mode and antisymmetric mode: (a) Flat layer layout structure; (b) Stagger layer layout structure; (c) Cross layer layout structure.

layer layout structure model is 1.012 GHz, and the characteristic frequency of the Mo electrode step layer layout structure model is 1.027 GHz.

Minifying the width of the interdigital electrode to reduce the wavelength of the SAW is beneficial to improve the working frequency of the SAW device. The characteristic frequency (f_F, f_S, f_C) curves of the three structures with the decrease of wavelength λ are shown in Figure 4. When using the initial structural parameters, the characteristic frequency relationship of the three structures is $f_F > f_S > f_C$. With the decrease of λ, the characteristic frequencies of the three structures are significantly improved, and the increase is consistent. When the λ is reduced from 4μm to 3μm, the characteristic frequency changes Δf_F, Δf_S, Δf_C of the three structures are increased by about 0.35 GHz.

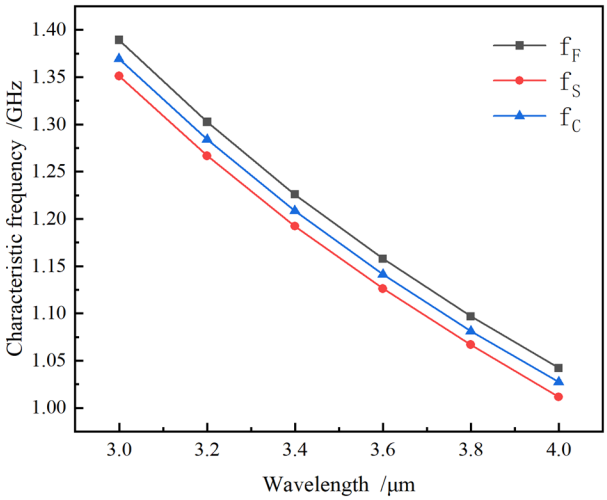

FIGURE 4. The variation of the characteristic frequency of the three layout structures with the wavelength.

B. NORMALIZATION INDEX OF FILM THICKNESS

Due to the dispersion of surface acoustic wave propagation in multilayer structure, it is necessary to consider the influence of film thickness normalization index on the characteristic frequency of multilayer structure SAW device. When $h_{DIA}/\lambda = 0.5$, the curves of the characteristic frequencies of the SAW devices with three different multilayer structures changing with the normalized exponent of h_{LN}/λ are shown in Figure 5.

When $h_{LN}/\lambda > 1$, the characteristic frequency of the SAW device with multi-layer piezoelectric film structure almost does not change with the decrease of h_{LN}/λ. This is because, during the propagation of SAW, the amplitude of the particle in the depth direction decays exponentially with the increase of depth, and most of the energy is concentrated in a wavelength depth range. SAW cannot penetrate the $LiNbO_3$ film

layer, and the coupling effect of the multi-layer structure almost disappears.

When $h_{LN}/\lambda < 1$, the characteristic frequency of the SAW device with multi-layer piezoelectric film structure increases significantly with the decrease of h_{LN}/λ, and the increased amplitude increases exponentially. When h_{LN}/λ is reduced from 0.8 to 0.7, the characteristic frequency of the three structures increases by 0.01 GHz; When h_{LN}/λ is reduced from 0.4 to 0.3, the increase of the characteristic frequency of the three structures has exceeded 0.2GHz. This is because SAW begins to penetrate the $LiNbO_3$ film layer at this time, and the penetration depth is further enhanced with the decrease of the penetration depth. SAW is more concentrated on the two-way propagation at the interface between the $LiNbO_3$ film layer and the Diamond film layer. The high sound velocity characteristics of the Diamond film layer begin to affect the propagation of SAW, that is, the coupling characteristics of the multilayer structure are enhanced with the decrease of the normalized index.

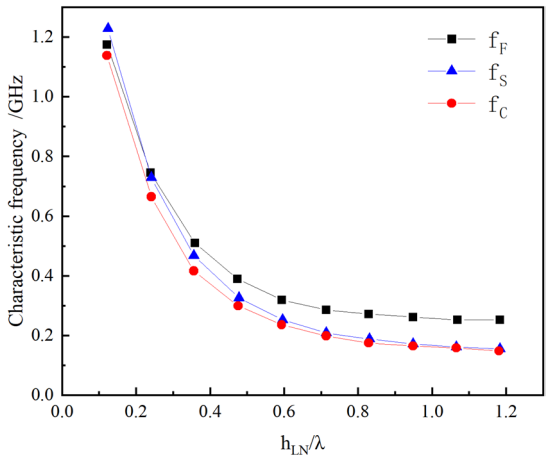

FIGURE 5. The characteristic frequencies of the three layout structures change with h_{LN}/λ.

When $h_{DIA}/\lambda = 0.5$, $h_{DIA}/\lambda = 0.7$, $h_{DIA}/\lambda = 1$, the characteristic frequencies of three different structures change with h_{LN}/λ as shown in Figure 6. It can be found that for SAW devices with the same multi-layer structure, changing the normalized index of the Diamond film layer will not have a significant effect on the characteristic frequency of the multi-layer piezoelectric film structure.

C. ELECTROMECHANICAL COUPLING COEFFICIENT

The electromechanical coupling coefficients of the three multi-layer structures under different conditions change with h_{LN}/λ as shown in Figure 7.

When $h_{LN}/\lambda \geq 0.5$, no matter how h_{DIA}/λ changes, the electromechanical coupling coefficient K_F^2 of the IDT flat layer layout structure does not change significantly; When $h_{LN}/\lambda < 0.4$, the influence of h_{DIA}/λ suddenly becomes obvious. When $h_{DIA}/\lambda = 0.3$, K_F^2 increases sharply and reaches 11.7 %, which is significantly higher than 5.5 % of the commonly used cut type of $LiNbO_3$ single crystal [20].

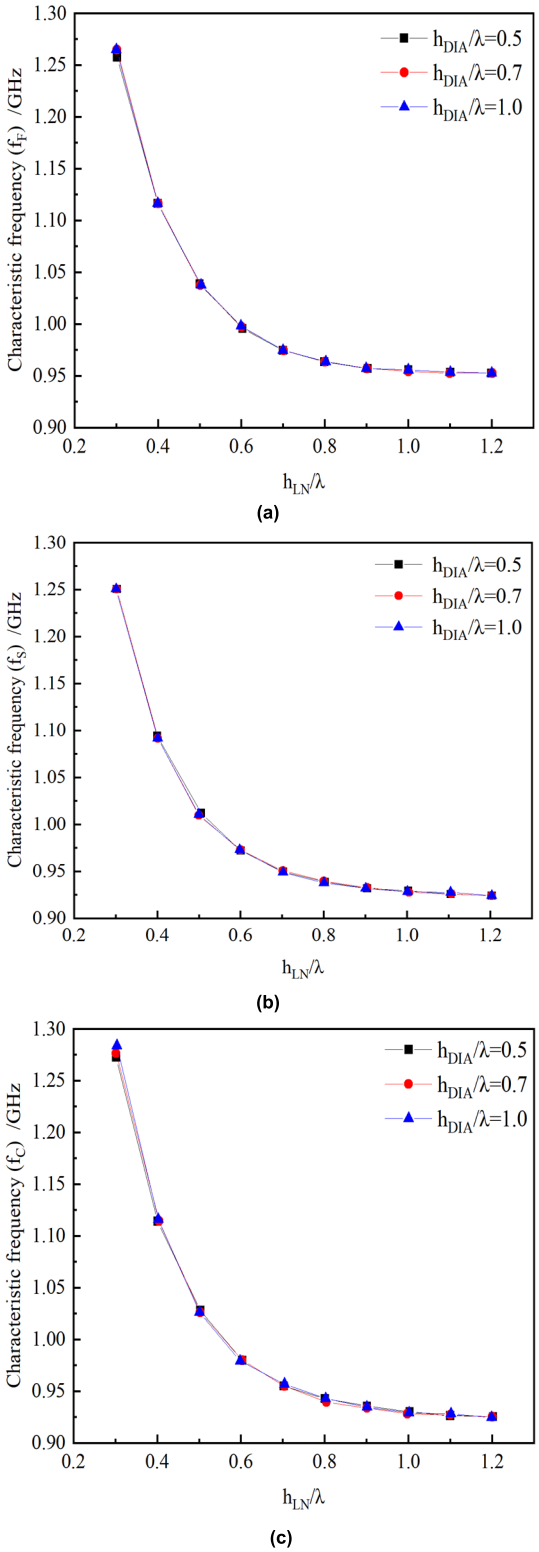

FIGURE 6. The change of the characteristic frequency of the three layout structures with h_{LN}/λ under different conditions: (a) Flat layer layout structure; (b) Stagger layer layout structure; (c) Cross layer layout structure.

The electromechanical coupling coefficient of IDT stagger layer layout structure has a good consistency with the normalized parameter of $LiNbO_3$ film thickness. When

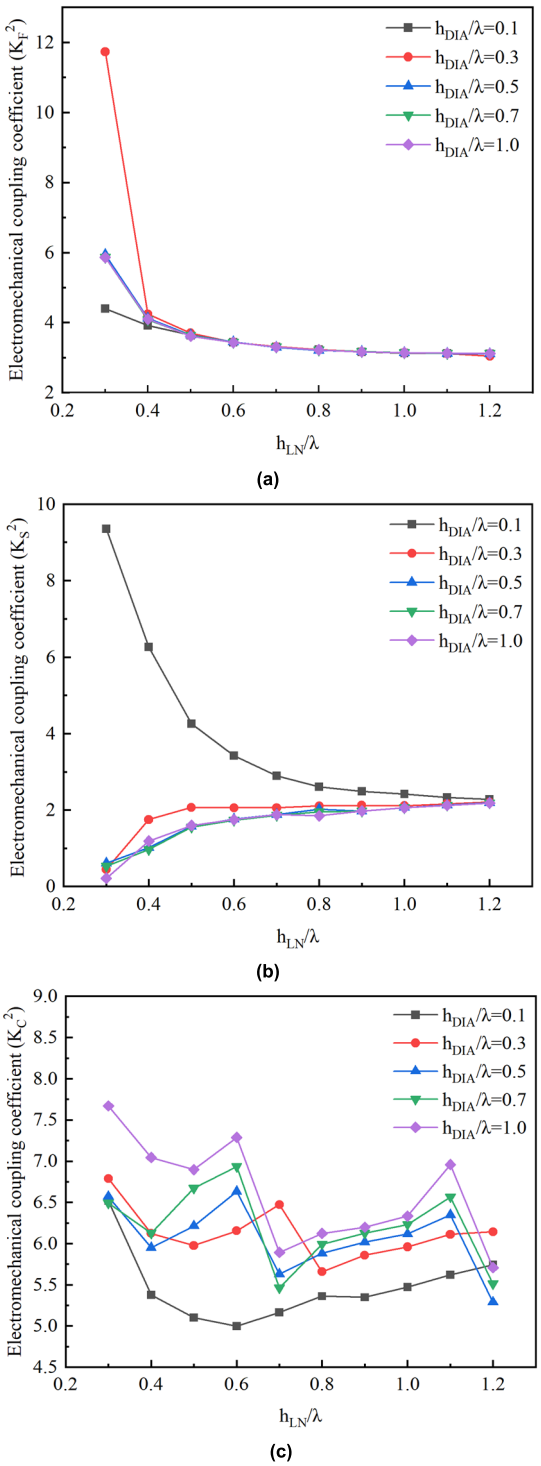

FIGURE 7. The change of electromechanical coupling coefficient of the three layout structures with h_{LN}/λ under different conditions: (a) Flat layer layout structure; (b) Stagger layer layout structure; (c) Cross layer layout structure.

$h_{DIA}/\lambda > 0.1$, K_S^2 decreases with the decrease of h_{LN}/λ; when $h_{DIA}/\lambda = 0.1$, K_S^2 increases with the decrease of h_{LN}/λ; when $h_{DIA}/\lambda = 0.1$ and $h_{LN}/\lambda = 0.3$, K_S^2 reaches 9.35%.

There is no obvious consistency between the electromechanical coupling coefficient of the IDT structure and the normalized parameters of the $LiNbO_3$ film thickness, and most of them fluctuate in the range of 5 % to 7.5 %.

D. DIFFERENT MO ELECTRODE ARRANGEMENT FORMS

As the excitation and receiving device of SAW, the structural characteristics of IDT directly affect the propagation characteristics of SAW. When the IDT material is determined, the finger width is 0.25 times the wavelength for uniform IDT, so the electrode thickness becomes an important parameter affecting the SAW propagation characteristics. In addition, the distance between IDT electrodes with different polarities is a fixed value in the simulation process, but in the actual preparation of SAW devices, it is a range value. Therefore, this section mainly discusses the influence of different electrode thicknesses and electrode spacing on SAW propagation characteristics.

1) ELECTRODE THICKNESS

The curve of the characteristic frequency of the three multi-layer structures with the change of h_{IDT}/λ is shown in Figure 8. When $h_{IDT}/\lambda \geq 0.1$,there is $f_F < f_S < f_C$. With the decrease of h_{IDT}/λ, the characteristic frequencies of the three structures begin to increase gradually; when $0.07 < h_{IDT}/\lambda < 0.1$,there is $f_S < f_F < f_C$; when $h_{IDT}/\lambda = 0.07$, there is $f_S < f_C < f_F$.

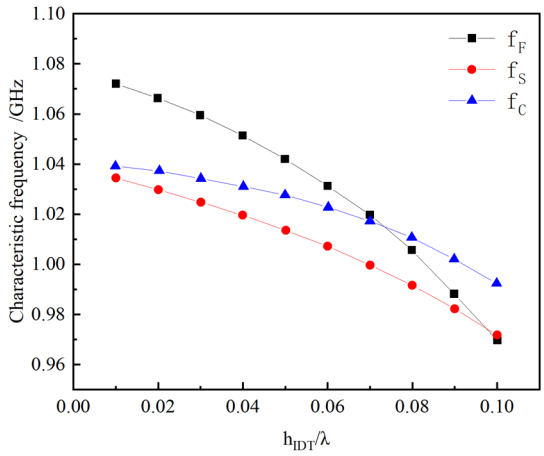

FIGURE 8. The change of the characteristic frequency of the three layout structures with h_{IDT}/λ.

The curve of electromechanical coupling coefficient of the three multi-layer structures with the change of h_{IDT}/λ is shown in Figure 9. It can be seen that K_F^2, K_S^2 and K_C^2 increase with the increase of h_{IDT}/λ, when $h_{IDT}/\lambda = 0.1$, K^2 of IDT flat layer layout structure exceeds 20 %.

It can be seen that the influence of the value of h_{IDT}/λ on the characteristic frequency and the electromechanical coupling coefficient is contradictory. If the characteristic frequency is increased, the K^2 of the device will be reduced. The thin IDT electrode is difficult to process and is easy to break because it cannot withstand the fatigue and high temperature caused by high-frequency mechanical vibration. Increasing the thickness will bring an obvious mass-loading

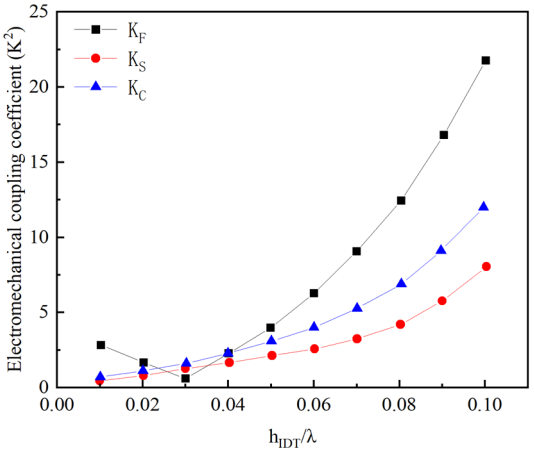

FIGURE 9. The change of electromechanical coupling coefficient of the three layout structures with h_{IDT}/λ.

effect to the piezoelectric film. Therefore, when designing the specific structural parameters of the device, it is necessary to comprehensively consider various factors.

2) ELECTRODE SPACING

The distance between the positive and negative IDT electrodes cannot be guaranteed to be equal during the preparation of the IDT electrode, so it changes within a range at the micro level. To solve this problem, the influence of the distance between the positive and negative electrodes of IDT on the propagation characteristics of SAW is analyzed by parametrically scanning the distance deviation value S_2 between the positive and negative IDTs. When S_2 is 0μ, it indicates that the distance between the positive and negative IDT electrodes is 1/4 wavelength, namely μ; When S_2 is $-\mu$, it indicates that the projections of positive and negative IDT on the bottom surface are in contact with each other, which is a short circuit for the IDT flat layout. When S_2 is $-\mu$, it indicates that the projections of positive and negative IDT on the bottom surface are completely coincident. The influence curves of the characteristic frequency and electromechanical coupling coefficient of the three IDT layout structures on the deviation of the positive and negative electrode spacing are shown in Fig 10.

As shown in Figure 10(a), the distance between the positive and negative electrodes of the IDT has no obvious effect on f_F for the IDT flat layer layout structure, K^2 decreases significantly with the decrease of the distance between the positive and negative electrodes of IDT. When the distance between the two reaches -0. μ, K_F^2 reaches the minimum, and then rises slowly.

As shown in Figure 10(b), the influence of the positive and negative electrode spacing deviation values on f_S and K_S^2 is just the opposite for the IDT stagger layer layout structure. The smaller the deviation value, the larger the K_S^2, and the higher the f_S, but the variation range of both is small.

As shown in Figure 10(c), the IDT cross layer layout structure is the least affected by S_2 among the three structures.

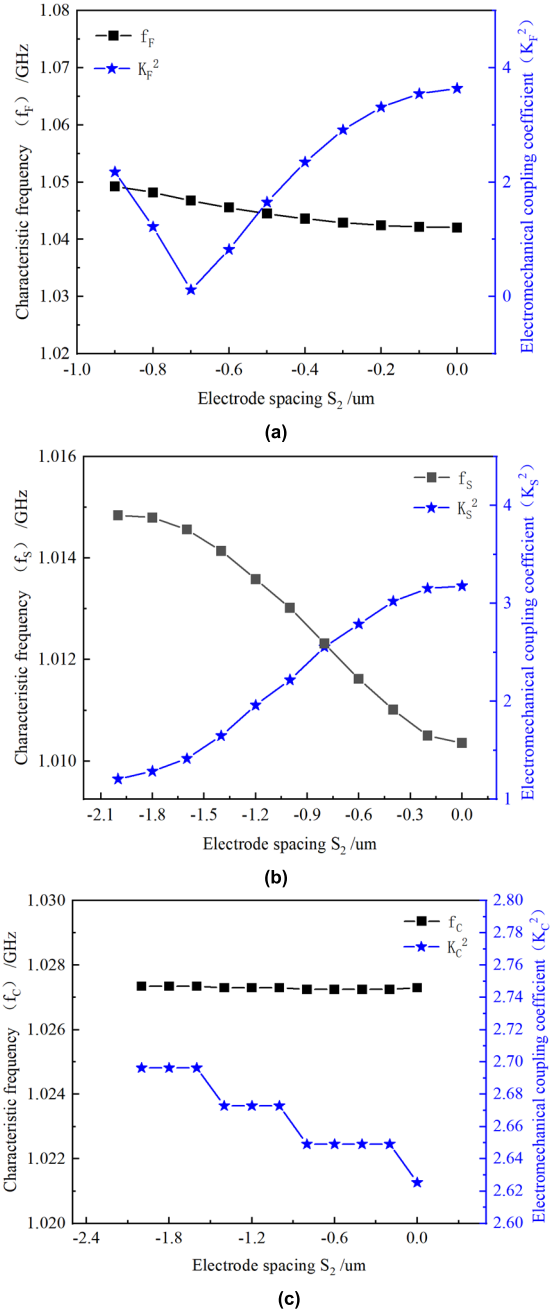

FIGURE 10. The f_0 and K^2 of the three IDT layout structures are affected by the positive and negative electrode spacing deviation: (a) Flat layer layout structure; (b) Stagger layer layout structure; (c) Cross layer layout structure.

It can be seen that f_C is almost no change, and K_C^2 is a slight increase with the decrease of S_2.

It can be found that the f_0 and K^2 of the flat layer layout structure and the stagger layer layout structure are greatly affected by S_2. Therefore, the IDT of these two structures needs to strictly control the process during the preparation, which can reduce the fluctuation range of S_2 and improve the repeatability of device fabrication.

Compared with the other two structures, the f_C and K_C^2 of the cross-layer layout structure is almost unaffected. Using

this feature, the spacing between the same layer electrodes can be shortened, and the operating wavelength and the overall structure size of the device can be reduced.

IV. CONCLUSION

(1) Based on $LiNbO_3$/Diamond/Si multilayer SAW devices, two IDT interdigital electrode parallel layout structures are designed. The IDT stagger layer layout structure is that the positive and negative electrodes of the interdigital electrodes are arranged on the top and bottom of the $LiNbO_3$ film layer respectively. The cross-layer layout structure of IDT is that the positive and negative electrodes of the interdigital electrode are arranged on the upper surface of the $LiNbO_3$ film layer and the lower surface of the Diamond film layer respectively.

(2) The variation of the characteristic frequency and electromechanical coupling coefficient of the two structures and the traditional flat-layer layout structure with wavelength and film layer normalization index is compared and analyzed. The results show that the performance of the multi-layer structure SAW device using the IDT stagger layer layout structure is more similar to the multi-layer structure SAW device using the IDT flat layer layout structure, but in the research direction of the miniaturization of the SAW device, the performance of the multi-layer structure SAW device using the IDT cross-layer layout structure is more stable.

REFERENCES

[1] D. Mandal and S. Banerjee, "Surface acoustic wave (SAW) sensors: Physics, materials, and applications," *Sensors*, vol. 22, no. 3, p. 820, Jan. 2022.

[2] A. Kumar and R. Prajesh, "The potential of acoustic wave devices for gas sensing applications," *Sens. Actuators A, Phys.*, vol. 339, Jun. 2022, Art. no. 113498.

[3] M. Mazalan, A. Noor, Y. Wahab, S. Yahud, and W. Zaman, "Current development in interdigital transducer (IDT) surface acoustic wave devices for live cell in vitro studies: A review," *Micromachines*, vol. 13, no. 1, p. 30, Dec. 2021.

[4] K. Suresh, V. Jeoti, S. Soeung, M. Drieberg, M. Goh, and M. Z. Aslam, "A comparative survey on silicon based and surface acoustic wave (SAW)-based RFID tags: Potentials, challenges, and future directions," *IEEE Access*, vol. 8, pp. 91624–91647, 2020.

[5] L. Wang, S. Chen, J. Zhang, D. Xiao, K. Han, X. Ning, J. Liu, Z. Chen, and J. Zhou, "Enhanced performance of 17.7 GHz SAW devices based on AlN/diamond/Si layered structure with embedded nanotransducer," *Appl. Phys. Lett.*, vol. 111, no. 25, Dec. 2017, Art. no. 253502.

[6] L. Qian, Z.-P. Wang, X.-J. Li, Y. Fei, and J. Zhao, "Design and optimization for double-sided interdigital transducer with piezoelectric substrate," in *Proc. 13th Symp. Piezoelectrcity, Acoustic Waves Device Appl. (SPAWDA)*, Harbin, China, Jan. 2019, pp. 1–4.

[7] W. Ziping, Q. Lei, F. Yue, C. Liangbin, and H. Donghui, "Research on the optimal design and application of wideband TIDT structure," *Rare Metal Mater. Eng.*, vol. 49, no. 11, pp. 3790–3795, 2020.

[8] Z. Wang, A. Zhou, D. Hao, J. Wang, and Y. Zhang, "Research on the sensing performance calibration of omni-directional broadband interdigital transducer based on PVDF substrate," *J. Intell. Mater. Syst. Struct.*, vol. 34, no. 1, pp. 79–88, Jan. 2023.

[9] Z. Li, X. Meng, B. Wang, and C. Zhang, "A three-dimensional finite element analysis model of SAW torque sensor with multilayer structure," *Sensors*, vol. 22, no. 7, p. 2600, Mar. 2022.

[10] S. Fan, W. Wang, X. Li, Y. Jia, Y. Sun, and M. Liu, "Optimization of AIN composite structure based surface acoustic wave device for potential sensing at extremely high temperature," *Sensors*, vol. 20, no. 15, p. 4160, Jul. 2020.

[11] Q. Zhang, Z. Chen, Y. Chen, J. Dong, P. Tang, S. Fu, H. Wu, J. Ma, and X. Zhao, "Periodic analysis of surface acoustic wave resonator with dimensionally reduced PDE model using COMSOL code," *Micromachines*, vol. 12, no. 2, p. 141, Jan. 2021.

[12] L. Lei, B. Dong, Y. Hu, Y. Lei, Z. Wang, and S. Ruan, "High-frequency surface acoustic wave resonator with diamond/AlN/IDT/AlN/diamond multilayer structure," *Sensors*, vol. 22, no. 17, p. 6479, Aug. 2022.

[13] J. Shen, J. Luo, S. Fu, R. Su, W. Wang, F. Zeng, C. Song, and F. Pan, "3D layout of interdigital transducers for high frequency surface acoustic wave devices," *IEEE Access*, vol. 8, pp. 123262–123271, 2020.

[14] E. Bausk, E. Kolosovsky, A. Kozlov, and L. Solie, "Optimization of broadband uniform beam profile interdigital transducers weighted by assignment of electrode polarities," *IEEE Trans. Ultrason., Ferroelectr., Freq. Control*, vol. 49, no. 1, pp. 1–10, Jan. 2002.

[15] L. Gao and W. Lu, "Surface acoustic wave type electrode-area-weighted wavelet inverse-transform processors with phase compensation," *IET Circuits, Devices Syst.*, vol. 11, no. 6, pp. 624–630, Nov. 2017.

[16] W. Lu, L. Gao, and J. Zhang, "A novel electrode-area-weighted method of implementing wavelet transform processor with surface acoustic wave device," *Int. J. Circuit Theory Appl.*, vol. 44, no. 12, pp. 2134–2146, Dec. 2016.

[17] F. Bénédic, M. B. Assouar, P. Kirsch, D. Monéger, O. Brinza, O. Elmazria, P. Alnot, and A. Gicquel, "Very high frequency SAW devices based on nanocrystalline diamond and aluminum nitride layered structure achieved using e-beam lithography," *Diamond Rel. Mater.*, vol. 17, nos. 4–5, pp. 804–808, Apr. 2008.

[18] V. Mortet, O. A. Williams, and K. Haenen, "Diamond: A material for acoustic devices," *Phys. Status Solidi (A)*, vol. 205, no. 5, pp. 1009–1020, May 2008.

[19] S. I. Shikata, A. Hachigo, H. Nakahata, and M. Narita, "Simulation of characteristics of a $LiNbO_3$/diamond surface acoustic wave," *IEEE Trans. Ultrason., Ferroelectr., Freq. Control*, vol. 51, no. 10, pp. 1308–1313, Oct. 2004.

[20] R. Lu and S. Gong, "RF acoustic microsystems based on suspended lithium niobate thin films: Advances and outlook," *J. Micromech. Microeng.*, vol. 31, no. 11, Nov. 2021, Art. no. 114001.

XU MENG was born in Harbin, Heilongjiang, China, in 1988. He received the bachelor's and master's degrees in vehicle engineering and the Ph.D. degree in vehicle application engineering from Northeastern Forestry University, in 2011 and 2023.

From 2013 to 2016, he was an Assistant Lecturer with Heilongjiang Oriental College. Since 2023, he has been a Lecturer with Changzhou Institute of Technology. He has written over ten articles and over ten inventions. His research interests include intelligent sensors and autonomous driving technology.

ZHIPENG LI was born in Harbin, Heilongjiang, China, in 1963. He received the Ph.D. degree in mechanical engineering from Northeast Forestry University, in 2008.

He is currently a Professor with the School of Mechanical and Electrical Engineering, Northeast Forestry University. He presided over two projects funded by China Natural Science Foundation. He have written over 80 journal articles and over 60 patents.